Comparison and Modeling of Commercial Supercapacitors via Standardized Potentiostatic Electrochemical Impedance Spectroscopy

Filippo Gherdovich, Giuseppe Taddia, Sandro Maria Tenconi, Miguel Pretelli, Alessandro Lampasi, Francesca Soavi, and Maria Luisa Di Vona

Abstract The main scope of the study is the characterization of the capacitive and resistive behavior of two supercapacitor cells and one hybrid supercapacitor available on the market, through potentiostatic electrochemical impedance spectroscopy (PEIS). The PEIS tests were performed by applying to all cells the same voltage perturbation in the same frequency range. In a first phase, the instrumentation used for the acquisitions was optimized, with particular care to the connections between the potentiostat and the supercapacitor cell. The Nyquist diagrams obtained for each sample are compared and capacitance/frequency graphs are deduced. The technological differences between various devices are then discussed in relation to the results. The characterization of the sample cells and the collected data are used to propose the corresponding models conceived for circuit simulation. These models are based on simple electronic components available in the standard circuit simulation software tools.

F. Gherdovich (✉) · G. Taddia · S. M. Tenconi · M. Pretelli
Energy Technology Srl, Bologna, Italy
e-mail: filippo.gherdovich@ocem.com; giuseppe.taddia@ocem.com; sandro.tenconi@ocem.com; miguel.pretelli@ocem.com

A. Lampasi
ENEA - Agenzia nazionale per le nuove tecnologie, l'energia e lo sviluppo economico sostenibile, Rome, Italy
e-mail: alessandro.lampasi@enea.it

F. Soavi
University of Bologna, Bologna, Italy
e-mail: francesca.soavi@unibo.it

M. L. Di Vona
University of Roma "Tor Vergata", Rome, Italy
e-mail: divona@uniroma2.it

W. Zamboni, G. Petrone (eds.), *ELECTRIMACS 2019*, Lecture Notes in Electrical Engineering 615, https://doi.org/10.1007/978-3-030-37161-6_51

1 Introduction

Potentiostatic electrochemical impedance spectroscopy (PEIS) is a powerful method of characterizing many electrical and electrochemical properties of materials and interfaces.

PEIS is useful to investigate the dynamics and kinetics of electric charges in the bulk or interface regions of any type of solid or liquid material (ionic, semiconductor, ion-electronic mixed, and even insulator). This non-destructive method was chosen to swiftly characterize the sample devices with defined low-voltage signals, in order to obtain electrical models from experimental results.

The general approach is to apply a sinus (perturbation voltage) around a DC voltage (Fig. 1) to the electrodes, ideally assuming that the properties of the electrode material do not change over time:

$$V(t) = V_{\mathrm{DC}} + V_{\mathrm{p}} \sin(\omega t) . \tag{1}$$

ω is the angular frequency. Induced current measured is:

$$I(t) = I_{\mathrm{DC}} + I_{\mathrm{p}} \sin(\omega t + \varphi) . \tag{2}$$

φ is the phase difference between $V(t)$ and $I(t)$. The expression of complex impedance is:

$$Z(i\omega) = \frac{V_{\mathrm{p}} \sin(\omega t)}{I_{\mathrm{p}} \sin(\omega t + \varphi)} = \mathrm{ESR} + \frac{1}{i\omega C} . \tag{3}$$

ESR is the equivalent series resistance of sampled device and C is its capacitance [1].

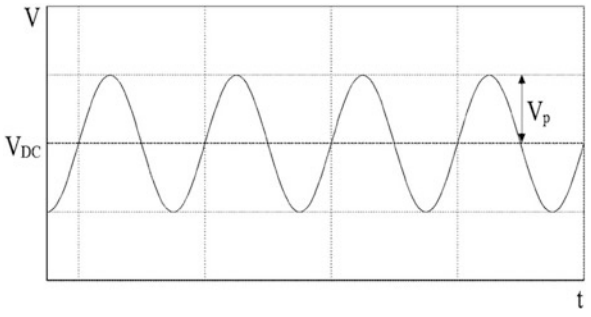

Fig. 1 Voltage over time during PEIS

2 Sample Cells Used for Tests

Three different commercial cells were tested [2]: two supercapacitors of about 3000 F (mentioned as "A" and "B") and a 3300 F hybrid supercapacitor, called "C". Table 1 reports the nominal characteristics of the three sample devices.

3 Preparation for the Test Optimization of Input/Output Cables

3.1 Test Instrumentation and Procedures

The measurement equipment includes:

- Five-channel PAR VSP galvanostat/potentiostat
- "EC-Lab V1023" software
- Four-terminal sensing cable
- Room temperature, 20 ± 1 °C
- Faraday cage

Table 1 Rated characteristics of the cells

Product specifications	Value
"A" cell	
Capacitance	3000 F
Voltage	2.7 V
ESR (DC)	0.29 mΩ
Specific energy	6 Wh/kg
Storable energy	3.04 Wh
Temperature range	[−40; 65] °C
"B" cell	
Capacitance	3200 F
Voltage	2.85 V
ESR (DC)	0.095 mΩ
Specific energy	6.8 Wh/kg
Storable energy	3.61 Wh
Temperature range	[−40; 70] °C
"C" cell	
Capacitance	3300 F
Voltage	3.8 V
ESR (DC)	1 mΩ
Specific energy	13 Wh/kg
Storable energy	6.62 Wh
Temperature range	[−30; 70] °C

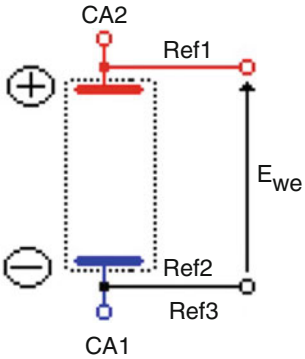

Fig. 2 Cell connection set-up (from EC-Lab V1023 software manual)

Test frequency range was set in the frame of 100 Hz–10 mHz, to focus interest on resistive-capacitive behavior of the sample, by applying a sinusoidal stimulus around the DC potential of 1 mV. DC is set to the cell open circuit voltage in the discharge state. The cell was placed in Faraday cage and connected to the potentiostat/galvanostat by five probes described in Fig. 2. The terminals CA1 and CA2 measured the current. The terminals REF1, REF2, and REF3 were used to measure the voltage. REF1 + CA2 were connected to the cell positive electrode. REF2, REF3, and CA1 were connected to the negative electrode. The PEIS voltage signal is controlled between REF1 and REF2 (REF2 and REF3, depicted in Fig. 2, are connected on the same electrode). The current is measured from CA2 to CA1. This cell connection was used for all the experiments reported below.

3.2 First Test with Hose Clamps

At first, hose clamps were used for the cell. The preliminary tests were performed on the supercapacitor "A".

Qualitatively, the tests give reliable results; however, quantitatively the cable connection included a stand-out resistance of around 22 mΩ, one order of magnitude higher than that reported by the manufacturer data sheet of cell "A", as shown in Table 1.

The obvious conclusion was to improve, first, the connections, by replacing the hose clamps on cell terminals with lugs. It was necessary to remove the plastic sheath, to which the clips, joined to hose clamps, were connected.

3.3 Test with Lugs

During this test, the above-described instrumentation and settings were unchanged, except for the connection to the supercapacitor terminals. Lugs were interposed between clips and cell terminals.

The resistance value obtained by this connection improved and decreased to 4.05 mΩ, 5 times less than the previous value obtained, but still 14 times the value declared by "A" manufacturer. This result showed that measurement connections are critical. Therefore, a further improvement of contact resistance was pursued.

3.4 Optimized Cable Design

Measurement wires were soldered directly to ring lugs. Keeping the test setting unchanged (except for PEIS AC that was set to 0.1 mV), the measured ESR reduced to 0.664 mΩ, 6 times less than the value obtained by lugs, but still about 2 times the value declared by "A" cell manufacturer.

Figure 3 reports the Nyquist plots obtained by PEIS run on cell "A" with the three different cable arrangements. The ESR corresponds to the high-frequency intercept on the real axis of the Nyquist plot.

4 Results and Interpretation of PEIS Tests

The following sections report the results of PEIS tests on the three commercial cells "A", "B", and "C" carried out by using optimized cables.

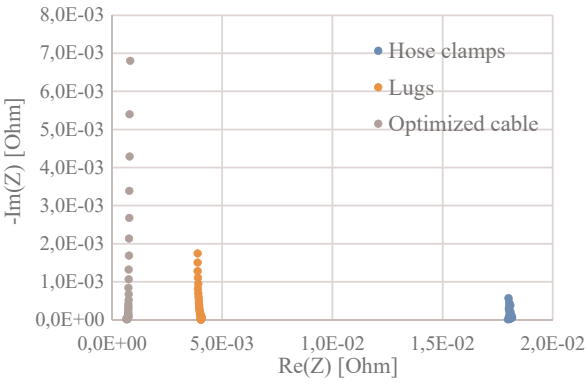

Fig. 3 Nyquist plots obtained from PEIS measurement of cell "A" with different connections

4.1 "A" Supercapacitor Cell

The impedance spectroscopy tests were conducted respecting the following test parameters:

- Initial frequency: 100 Hz
- Final frequency: 10 mHz
- AC voltage: 0.1 mV

The Nyquist diagram obtained from the PEIS test is shown in Fig. 4.

Each point in Fig. 4 corresponds to a specific frequency [3]. At the lower sampled frequency (0.01 Hz), the measured capacitance is equal to [4]:

$$C = \frac{1}{\omega \cdot \left[-\operatorname{Im}(Z)_{0.01\ \mathrm{Hz}}\right]} = 2340.5\ \mathrm{F}. \tag{4}$$

Cell "A" impedance response deviates from that of an ideal capacitor. Indeed, for an ideal capacitor, the Nyquist plot is a straight line parallel to the imaginary axis. In Fig. 4, the straight line has a slope (phase) <90°. This suggests a frequency dependence of capacitance that is highlighted by Fig. 5. The figure reports the capacitance vs. frequency Bode plot of cell "A". In Fig. 5, the capacitance decreases with the increase of the frequency. This has to be related to the diffusion rate of electrolyte ions through the porous architecture of the carbonaceous electrodes. At the lowest frequencies and lowest times, more charges can reach the porous interface, and then a higher capacitance is achieved. Consequently, in these conditions, the device stores more energy.

The curve in Fig. 5 can be fitted by a logarithmic function:

$$y = -308.1 \ln(x) + 1454.6 \tag{5}$$

For frequencies above 100 Hz, the behavior of the sample cell is inductive (see Fig. 10).

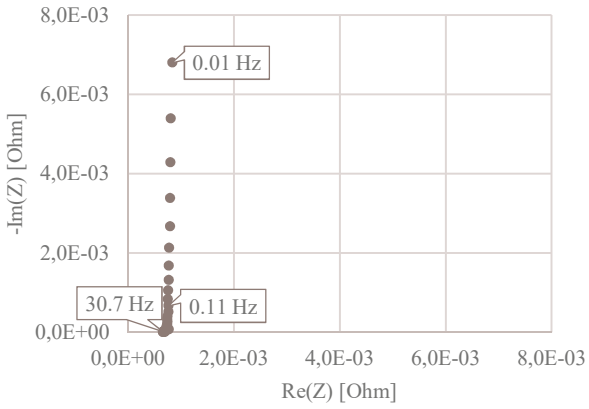

Fig. 4 Nyquist plot of cell "A." ESR is evaluated by the high-frequency intercept on the real impedance axis. The cell capacitance is obtained by the lowest-frequency imaginary impedance (see Eq. 4)

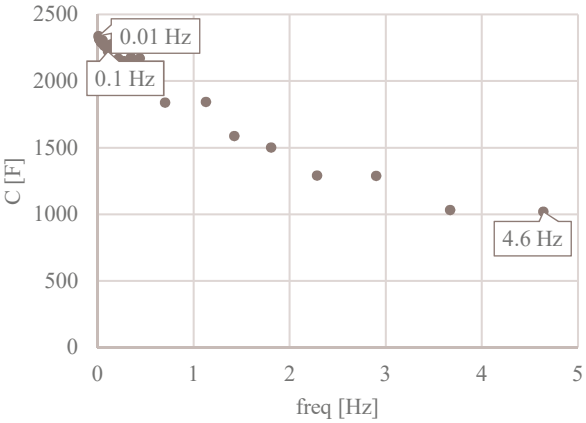

Fig. 5 Capacitance vs. frequency plot of cell "A"

4.2 "B" Supercapacitor Cell

The impedance spectroscopy tests were conducted by setting the following test parameters:

- Initial frequency: 100 Hz
- Final frequency: 10 mHz
- AC voltage: 0.25 mV

The connection to the terminals was harder because there is no thread for bolts on the terminals. As a rule, for very capacitive or low-impedance electrochemical systems, the potential amplitude can lead a current overflow that can stop the experiment in order to protect the unit from overheating. Using galvanostatic electrochemical impedance spectroscopy (GEIS), instead of PEIS, can avoid this inconvenient situation. The setback was solved reducing the perturbation voltage compared to the previous test. This was required for the lower internal resistance of "B" supercapacitor with respect to cell "A". Fig. 6 Nyquist plot of cell "B". ESR is evaluated by the high-frequency intercept on the real impedance axis. The cell capacitance is obtained by the lowest-frequency imaginary impedance (see Eq. 4). Figure 6 illustrates Nyquist diagram of "B" cell.

Basically, cell "B" Nyquist plot is similar to that of cell "A". The former mainly differs from that of the latter for the lower ESR. The value measured between the two frequency points 17–11 Hz is equal to 0.612 mΩ. The capacitive behavior starts to be appreciable at frequencies lower than 5 Hz. At the lower sampled frequency (0.01 Hz), the measured capacitance is equal to 2514 F, as shown in Fig. 6. Figure 7 reports the capacitance vs. frequency plot of cell "B".

Also for "B" cell, best fitting curve is gained with logarithmic equation:

$$y = -45.88 \ln(x) + 2337.1 \tag{6}$$

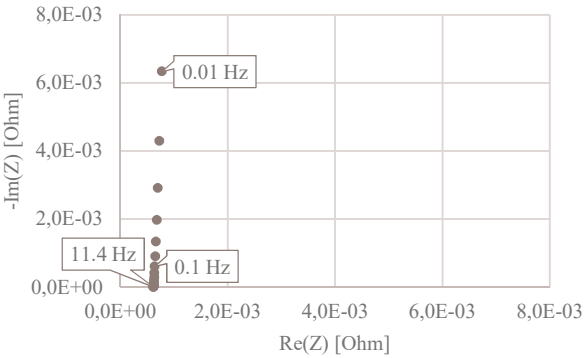

Fig. 6 Nyquist plot of cell "B." ESR is evaluated by the high-frequency intercept on the real impedance axis. The cell capacitance is obtained by the lowest-frequency imaginary impedance (see Eq. 4)

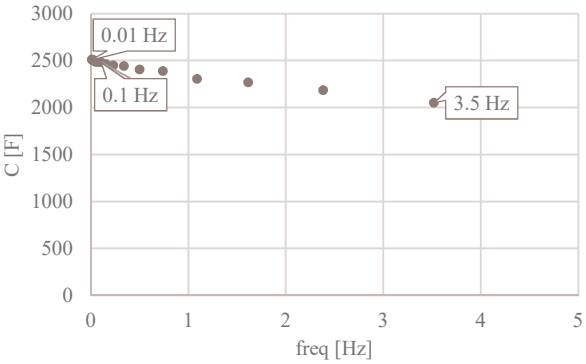

Fig. 7 Capacitance vs. frequency plot of cell "B"

4.3 "C" Hybrid Supercapacitor Cell

Unlike the two previous devices, the "C" cell is a lithium-ion capacitor (LIC). It is a hybrid supercapacitor composed of a pre-lithiated carbon anode, similar to a lithium-ion battery negative electrode. The positive electrode is an activated carbon, like for conventional supercapacitors [5]. The impedance spectroscopy tests were conducted setting the following test parameters:

- Initial frequency: 100 Hz
- Final frequency: 50 mHz
- AC voltage: 1 mV

The choice of a higher AC voltage is due to the fact that the cell has greater internal resistance than the "A" and "B" devices (Fig. 8). This gives no risk of over-current protections on the potentiostat.

The value of the measured series resistance is equal to 0.85 mΩ, similar to the nominal value (6 times as much).

In the "C" cell, due to its hybrid nature, the effect of electrolyte ion diffusion is more evident. Indeed, the low-frequency lines of the Nyquist plots significantly deviate from the ideal capacitor case discussed above. This is an important difference that acts as a watershed between the pure and the hybrid supercapacitor.

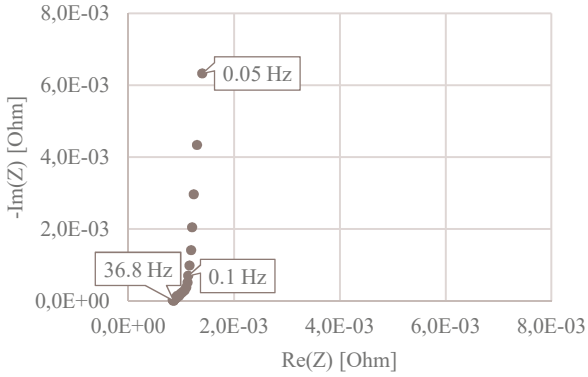

Fig. 8 Nyquist plot of cell "C." ESR is evaluated by the high-frequency intercept on the real impedance axis. The cell capacitance is obtained by the lowest-frequency imaginary impedance (see Eq. 4)

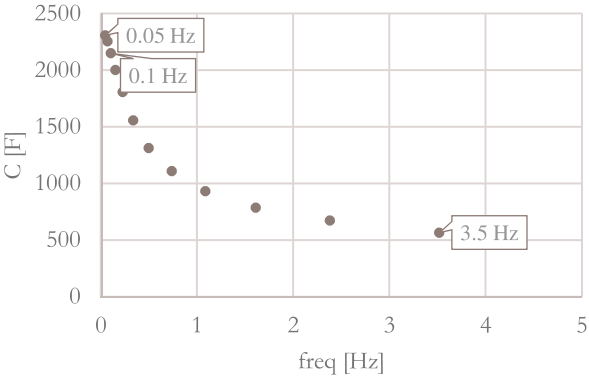

Fig. 9 Capacitance vs. frequency graph of the "C" sample cell

The ESR was evaluated at 54 Hz, while the capacitive behavior begun to be appreciated below 0.15 Hz. At the lowest sampled frequency (0.01 Hz), the measured capacitance was equal roughly to 2450 F (Fig. 9).

Behavior of hybrid cell acts as a power function:

$$y = 953.64x^{-0.343} \tag{7}$$

5 Test of Standardized Impedance Spectroscopy on All Three Devices

In order to be able to compare the "A", "B", and "C" sample cell behaviors, the following parameters have been "standardized":

- Initial frequency: 200 kHz
- Final frequency: 10 mHz
- AC voltage: 0.1 mV

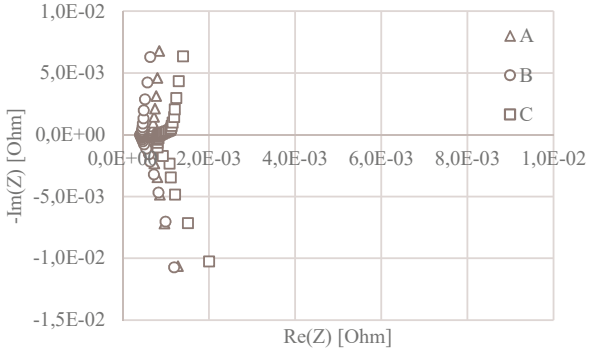

Fig. 10 Nyquist plots of cells "A," "B," and "C" obtained by standardized EIS test

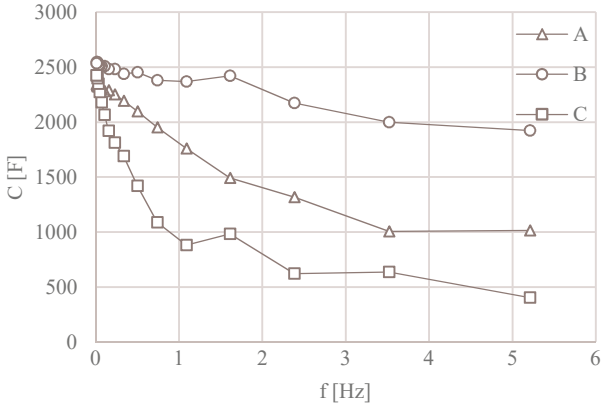

Fig. 11 Comparison of the capacitance vs. frequency trends of cells "A," "B," and "C" obtained by standardized EIS test

Figure 10 reports the Nyquist plots of the three cells and highlights that the three devices behave in approximately the same way. The main difference lies in the resistance of the device: the greater resistance of the "C" cell, where ion diffusion contribution is no longer negligible, stands out.

At the same time, the three cells' capacitance behaviors with frequency give different responses. This is evinced in Fig. 11 that compares the capacitance vs. frequency plots for the supercapacitor cells.

The cell "B" is the one with the highest performance, i.e., with the highest capacitance retention over the investigated frequency range. The corresponding plot has the lowest slope dC/df. In turn, the cell "C" (LIC, hybrid cell) features the lowest capacitance retention and the highest slope. The higher resistance value of cell "C" affects its power performance and its high-frequency energy response. In fact, cell "C" faradaic charge/discharge involves lithium-ion diffusion in the negative electrode, which is a slow process compared to the electrostatic charge/discharge of the conventional "A" and "B" cells.

6 Modeling Capacitive/Resistive Behavior Starting from Impedance Spectroscopy Tests

PEIS permits to convert experimental results in circuital model of energy storage device behavior. This is of paramount importance to address power electronics industrial needs. However, the non-linear behavior of supercapacitors makes modeling over a sufficiently wide frequency range difficult [6]. The application of supercapacitor models into software for electrical circuit simulation and design requires a realistic behavior of the component inside the simulated system. Implementation of the supercapacitor circuit model must take into account that many simulation software do not include elements like Warburg element, constant phase element (CPE), Gerischer element, etc. Given that supercapacitor capacitance is frequency dependent, it is suggested, in software developed considering CPE, to implement the Nyquist plot analysis substituting capacitance with these elements. CPE indeed takes into account how frequencies affect the imaginary component of impedance. Probably, the best way to connect experimental results with models applicable to electrical circuit simulator is to use the simplest electrical elements, remembering that the best circuit model is the simplest possible one, in order to achieve immediate results [7]. In case of supercapacitors, this means resistances, capacitors, and inductances. The kind of application determines the complexity of the model, and every element must have a physical meaning. Generally, supercapacitor could be represented by not more than five RC meshes, each one with different time constants [8]. Figure 12 depicts a solution for the resistive/capacitive behavior of analyzed supercapacitors samples.

A mono-branch model, $R_1 + R_2/C_1$, where R_1 is the device ESR while R_2 is self-discharge resistance, could represent "A" sample. C_1 is the capacitance between 0.01 and 100 Hz. In power electronic simulation, this model performs in a reliable manner not only supercapacitor cell dynamics but also modules. The self-discharge resistance can be inferred by the leakage current value that is often declared in the cell datasheet.

The best fit for "B" cell is achievable with a cogent structure model (Fig. 13).

Two RC meshes in series, $R_1/C_1 + R_2/C_2$, act as "B" supercapacitor cell. The first mesh has time constant $\tau_1 = 0.24$ ms, and the second mesh has $\tau_2 = 498$ s.

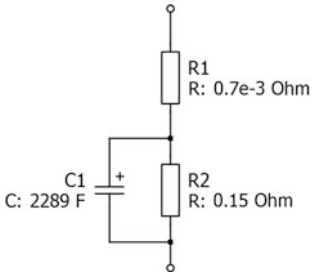

Fig. 12 Cell "A" equivalent circuit model

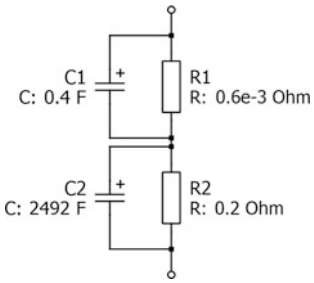

Fig. 13 Cell "B" equivalent circuit model

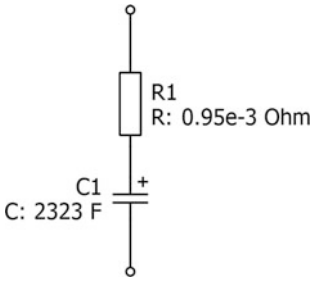

Fig. 14 Cell "C" equivalent circuit model

An overall behavior for "C" cell could be described by the equivalent circuit reported in Fig. 14.

"C" sample model described in Fig. 14 is not sufficiently representative of the hybrid cell. There is a way to improve fitting, but this implies the use of theoretical components such as Warburg element and so on. Indeed, an R(RC)W Randles circuit that takes into account the faradaic process occurring at the negative electrode should be used. Hybrid supercapacitors request further studies to be well modeled.

7 Conclusions

There is a difference of about 20% between the capacitance measured by PEIS and the results reported by the manufacturers of the tested supercapacitors. This difference may be related to the fact that the capacitance measurements were carried out without cell polarization (i.e., around 0 V).

It is generally recognized that the capacitance of the cells is partly voltage dependent: $C(V) = C_0 + kV$ [9]. Rated capacitances are generally meant with the charge at full voltage. This might explain the difference. Also, datasheet capacitance values are obtained by different techniques. Typically they result from galvanostatic tests.

Concerning the ESR, the values that we obtained by PEIS are 5–6 times higher than the values declared by the manufacturers. This is probably due to the extremely low values of the resistance to be measured, at the lower limit of the available instruments.

As said in the introduction, many other tests, such as charge-discharge test, must endorse models obtained by PEIS. To enlarge supercapacitor knowledge, it is useful to apply PEIS test also for supercapacitor modules, identifying right instrumentation.

Acknowledgments Thanks go to professors John R. Miller (Case Western Reserve University) and Philippe Knauth (Aix-Marseille Universitè) for their suggestions and willingness.

References

1. M. Grossi, B. Riccò, Electrical impedance spectroscopy (EIS) for biological analysis and food characterization: a review. J. Sens. Sens. Syst. **6**, 303–325 (2017)
2. F. Rafik, H. Gualous, R. Gallay, A. Crausaz, A. Berthon, Frequency, thermal and voltage supercapacitor characterization and modeling. J. Power Sources **165**, 928–934 (2007)
3. W. Lajnef, J.-M. Vinassa, O. Briat, S. Azzopardi, E. Woirgard, Characterization methods and modelling of ultracapacitors for use as peak power sources. J. Power Sources **168**, 553–560 (2007)
4. P. Navalpotro, M. Anderson, R. Marcilla, J. Palma, Insights into the energy storage mechanism of hybrid supercapacitors with redox electrolytes by Electrochemical Impedance Spectroscopy. Electrochim. Acta **263**, 110–117 (2018)
5. J. Zhang, J. Wang, Z. Shi, Z. Xu, Electrochemical behavior of lithium ion capacitor under low temperature. J. Electroanal. Chem. **817**, 195–201 (2018)
6. S.V. Rajania, V.J. Pandya, V.A. Shah, Experimental validation of the ultracapacitor parameters using the method of averaging for photovoltaic applications. J. Energy Storage **5**, 120–126 (2016)
7. N. Mohan, T.M. Undeland, W.P. Robbins, *Power Electronics: Converters, Applications and Design* (Wiley, New Delhi, 2017)
8. L. Zhang, X. Hu, Z. Wang, F. Sun, D.G. Dorrell, A review of supercapacitor modeling, estimation, and applications: a control/management perspective. Renew. Sustain. Energy Rev. **81**, 1868–1878 (2018)
9. L.E. Zubieta Bernal, *Characterization of Double-Layer Capacitors for Power Electronics Applications*, Master of applied science thesis, University of Toronto, 1997